Ecological Questions 36 (2025) 3: 137–150 http://dx.doi.org/10.12775/EQ.2025.024

Sea Surface Temperature Dynamics and Seasonal Forecasts based on ARIMA Modelling for the Indian Ocean using MODIS Satellite Data (2002–2020)

Imran Ahmed Khan[1,*], Altaf Hussain Lahori[2], Hossein Vahidi[3], Mudassar Hassan Arsalan[4], Muhammad Haroon Shaukat[5], Sana Ilyas[6], Ibrahim Zia[7]

[1] Department of Geography, University of Karachi, Karachi 75270, Pakistan
[2] Department of Environmetal Sciences, Sindh Madressatul Islam University, Karachi 74000, Pakistan
[3] Department of Geography, Faculty of Letters and Humanities, Ferdowsi University of Mashhad, Mashhad 91779-48974, Iran
[4] School of Computing, Engineering and Mathematics, Western Sydney University, Australia
[5] Department of Statistics Quid e Azam University, Islamabad, Pakistan
[6] Department of Ecology, Tashkent Institute of Irrigation and Melioration, Tashkent, Uzbikistan
[7] National Institute of Oceanography, ST.47, Block 1, Clifton, Karachi 2E8, Pakistan
* Corresponding author email: imranak32@uok.edu.pk (I.A.K)

Received: 10 October 2024 / Accepted: 3 June 2025

Abstract. Understanding global climate change patterns and high-risk areas is vital for effective monitoring and forecasting. This study focuses on the assessment of Sea Surface Temperature (SST), a critical factor in climate dynamics, particularly in the delicate Indian Ocean region, which significantly influences the global climate system. We analyze the spatial and temporal patterns of SST from August 2002 to April 2020, encompassing the Arabian Sea to the central Indian Ocean. Utilizing MODIS Aqua Monthly SST data from the Ocean Color platform, we examine seasonal, annual, and intra-annual SST variations. Our analysis includes evaluating anomalies, standard anomalies, coefficients of variation, and time series, employing seasonal autoregressive integrated moving average (SARIMA) modeling for short-term forecasting. Results indicate an overall upward trend in SST, characterized by a bi-modal pattern annually and notable variations in monthly averages. The SARIMA model has effectively predicted SST values up to April 2023. This research addresses five primary concerns: estimating spatio-temporal SST patterns in the Indian Ocean, analyzing normal and standardized anomalies, assessing monthly and yearly variations, applying SARIMA for SST prediction, and detecting climate change signatures through decadal rising patterns. These findings highlight the value of satellite data for monitoring marine climate and supporting decisions in environmental management and fisheries. Regional SST analysis is key to understanding local warming and mitigating ecological risks.

Keywords: Ocean remote sensing, SST, Indian Ocean climate, Ocean color SST, Inter-annual variability.

1. Introduction

Sea surface temperature provides vital information on the global climate system. Since oceans cover 71% of Earth's surface, researchers monitor SST to understand its interaction with the climate (Embury et al., 2024). Sea surface temperature (SST) is an important character for analyzing marine ecology and global climate. Ocean conditions and hydro-climate variability could be assessed with long-term SST data, as noted by (Khan et al., 2015). This information is

notable for the prediction of climate and its variation. It has a direct impact on ocean biology and species distribution. SST also acts as an indicator for monitoring and observing marine disasters (Kilpatrick et al., 2015). Sea surface temperature (SST) is deemed as one of the important oceanographic parameters in climate and ocean studies, as observed by (Rayner et al., 2003). It is considered a vital climate variable, because it influences many physical, chemical, and biological properties of oceans and is an effective indicator of variances in marine ecosystems (McWilliams et al., 2005). The SST spatial circulation globally is valuable in the area of warm fronts, ebb and flow frameworks in the seas, and the trading of warm vitality between the sea and the atmosphere, as stated by (Saeedi et al., 2019). SST is a crucial parameter in weather prediction and atmospheric model simulations and is also important for the study of marine ecosystems (Karagali et al., 2012).

Global warming correlated with anthropogenic climate change results in both increased mean values of SST and changes in thermal atmospheric processes that affect ocean circulations (Ji et al., 2018). It also influences the physiology, behavior, and demographic aspects of organisms, altering size, structure, range of distribution, and abundance of populations, consequently producing changes in the trophic programs and the community functions of ecosystems (Beaugrand, 2004). Changes in SST lead to alterations in marine biological processes, from individuals to ecosystems, at local to global scales, affecting ecosystem services (Osborne et al., 2020). The ocean plays a fundamental role in moderating climate change by serving as a major heat and carbon sink (Pastor et al., 2019). The global ocean is already experiencing notable influences of climate change and its accompanying effects (Hill, 2020). These changes involve air and water temperature warming, seasonal shifts in species, coral bleaching, and other significant ecological impacts (Choi et al., 2019). Furthermore, we can expect more extreme weather events (droughts, floods, storms), which will impact both habitats and species (Harrison et al., 2017).

Remote sensing technologies provide exceptional services, including regional-level resource mapping with temporal coverage. With GIS tools, remotely sensed data has been integrated for precise scientific measurement and modeling (Minnett et al., 2019). The world is now witnessing phenomena through geo-informatics that were previously impossible to observe. The acquisition of SST data began in the late 1980s using infrared bands. Since then, satellite images have become invaluable for temporal and spatial assessments of SST. NASA's Terra and Aqua satellites, launched with the MODerate-resolution Imaging Spectroradiometer (MODIS) in 1999 and 2002, respectively, have played a significant role in this effort (Savtchenko et al., 2004). SST from MODIS has provided consistent time-series data with global coverage and various temporal resolutions (Minnett et al., 2004). MODIS calculations are of higher value than other remotely sensed data for ocean information extraction (Salomonson et al., 2002). For SST measurement, multispectral thermal IR measurements from space use emitted radiances at wavelengths such as mid-wave (3–6 μm) and thermal IR regions of the electromagnetic spectrum. To minimize atmospheric noise (from gases and particles like H_2O and CO_2), these radiance values are converted to Brightness Temperature (Tb). Atmospheric correction is then applied for accurate assessments. For MODIS data, SST is presented in product form (Quan-jun, 2009; Gladkova et al., 2016).

The goal of this study was to create SST spatial patterns and temporal variations in the Northern Indian Ocean by using MODIS data from 2002 to 2020. This information is particularly important for the conservation and supervision of marine resources of the region. Therefore, this study is to construct two decadal SST dynamics to advance our perception of climate and its variability and possible impacts on ocean ecosystems through Time series and trend analysis. The Adopted methodology is not new but significant in terms of regional coverage and duration.

2. Materials and Methods

2.1. Study area

The study area is a part of Indian Ocean bordered with India, Pakistan and Arabian Peninsula in the east, north and west respectively with the extent ranging from 5°S to 31°N in latitude and, 30 to 83° E in longitude (Figure 1). The region of interest also covers the Gulf of Persia, Oman and Aden along with Red Sea, and Gulf of Kutch. Some significant deep-sea ports are also located in this region (Malik, 2012).

2.2. MODIS Data

MODIS datasets can be accessed from several platforms one of that is Ocean Color (He et al., 2009). MODIS Aqua dataset was downloaded from the ocean color website from Ocean Biology Processing Group (OBPG) at NASA's Goddard Space Flight Center (https://oceancolor.gsfc.nasa.gov) for 19 years (August, 2002 – April, 2020). The MODIS Aqua contains SST level 3 with a 4 km daytime product resolution. The geophysical variable information of SST has been extracted using this MODIS Aqua dataset which has been projected on a spatial grid over a defined period. Each file holds an equi-rectangular projection and registration of structured square cells grids based on a grid of floating-point values for a single parameter has been plotted as a preprocessing step. NASA-

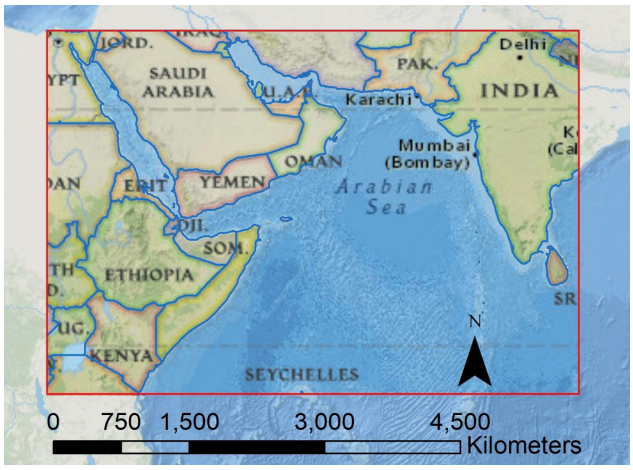

Figure 1. Study area

standard processing and distribution of the SST products from the MODIS sensors are conducted, using software developed by the Ocean Biology Processing Group (OBPG) (Nandkeolyar et al, 2013; Raitsos et al, 2013). The details of the stepwise process has been illustrated in Figure 2.

2.3. Research Design

The MODIS based SST images were processed to develop a time series database of 213 months from August 2002 to April 2020. The level 3 data is geometrically corrected to clear the data from orbit overlap and swath distortions. The dataset was acquired in in NetCDF format. Detailed statistics for these data sets have been evaluated and analyzed after converting into GeoTiff in ArcGIS interface. The R program has been utilized for seasonal, annual and intra-annual analysis and also employed for time series ARIMA model, etc.

2.3.1. Temperature anomaly and Standardize anomaly

Climate change analysis mostly utilizes temperature anomalies (Nandkeolyar et al., 2013), which is calculated through long-term temperature average as a reference value with current temperature values. The anomaly identifies the rate of change or difference between the expected and the currently values. A hotter or cooler temperature than the normal average would be expressed in terms of negative or positive anomalies respectively (Equation 1).

$$a_i = x_i - \mu \quad (1)$$

where,
a_i = Anomalies
x_i = Monthly temperature
μ = Mean Monthly temperature.

Normalized anomalies, likewise alluded to as standardized anomaly is calculated by dividing the anomalies with standard deviation values of the climatic variables (Equation 2). Standardized anomaly generally provides more information about the magnitude of the change as the influences of dispersion have been removed.

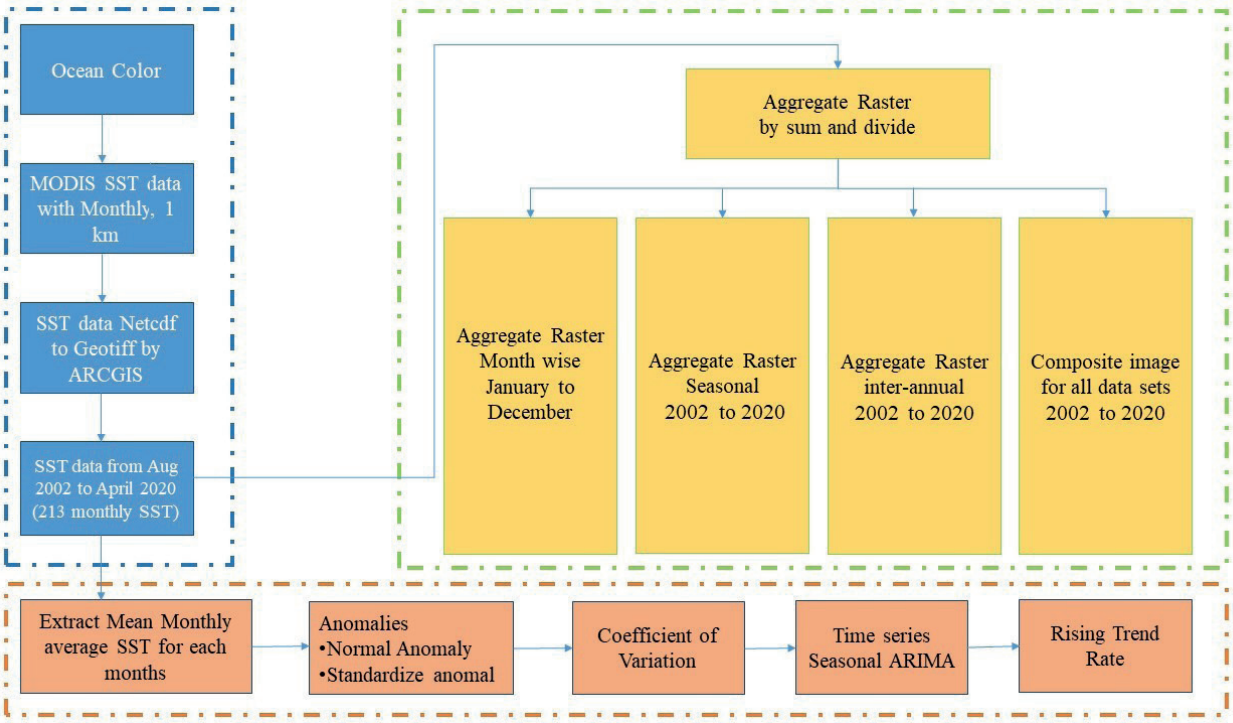

Figure 2. Flow chart of the study

$$a_i^n = \frac{x_i - \mu}{\sigma} \quad (2)$$

where:
a_i^n = Standardized Anomalies
X_i = Monthly temperature
μ = Mean Monthly temperature
σ = Standard Deviation of all data.

This removes any dispersion in the data which makes comparisons between different variables more appropriate.

2.3.2. Coefficient of Variation

The coefficient of variation, also recognized as relative standard deviation, is a standardized measure of the dispersion of a probability distribution or frequency distribution. It is frequently communicated as a percentage and is characterized as the ratio of the standard deviation to the mean (Nandkeolyar et al., 2013). The coefficient of variation (CV) provides the scale of the monthly, seasonal, and inter annual variability between temperature records for the specified time period.

CV = coefficient of variation $CV = \frac{\sigma}{\mu}$ (3)

where:
μ= Mean Monthly temperature
σ = Standard Deviation of all data.

2.3.3. Time series and ARIMA Modelling for forecasting

Time series modeling has proved its usefulness in various fields including meteorology, and climate change studies. It employs useful information from historical datasets and extracts relevant data to develop a model to recreate different cycles (Ye et al., 2013).

Among the statistical models available, considerable interests lies with linear and multiple regression models, trend modeling, averages, probability distributions, analysis of canonical correlations, ARIMA, SARIMA, and Principal Component Analysis (PCA) (Goswami et al., 2017). ARIMA (Auto Regressive Integrated Moving Average) or Seasonal Autoregressive Integrated Moving Average – SARIMA models are the most successful linear model for forecasting a seasonal time series. An Auto Regressive Integrated Moving Average -ARIMA is a descriptive examination model that utilizes time dependent information to either better comprehend the informational index or to anticipate future patterns. The ARIMA methodology has been widely used for modeling and predicting the behavior of temporal series of observations for various variables (Chen et al., 2018).

Over the last 30 years, ARIMA models have gained popularity for forecasting (Box & Jenkins, 1970), particularly in climatological and environmental studies (Putra et al., 2019). ARIMA works by objectively constructing a model based on past time series observations to predict future values of the series. It involves three control constants (pattern, occasion, and unpredictable impact) that regulate the effects of time division over a specific period (Shehhi & Kaya, 2020). ARIMA has been employed for assessing short-term forecasts in areas such as fisheries and forestry, as well as predicting droughts, forest fires, and the prognosis of tree diseases while observing ocean and coastal changes (Alonso et al., 2019).

The SARIMA model of Box and Jenkins is generally denoted as ARIMA (p, d, q) × (P, D, Q) where the commonly used three types of parameters (p, d, q) represents the autoregressive (p); differencing (d) and moving average parameters (q) (Mishra and Desai, 2005). In the standard notation "p–d–q", a model described as (0, 1, 2) means that it contains 0 (zero) autoregressive (p) parameters and 2 moving average (q) parameters which were computed for the series after it was differenced once (d = 1).

2.3.4. Seasonal Autoregressive Integrated Moving Average (SARIMA) Model

Box et al. (1994), present a general multiplicative (SARIMA) model, as an extension of ARIMA (Box et al., 1994), which deals with both seasonal and non-seasonal time series. The SARIMA model is consists of two parts such as (p, d, q) and (P, D, Q) represent non-seasonal and seasonal part respectively. Two separate equations of the non-seasonal and seasonal part are as follows (Chen et al., 2009).

$$\psi_p(\beta)\nabla^d z_t = \gamma_q(\beta)d_t \quad \textbf{(4)}$$

$$\phi_p(\beta^s)\nabla_s^D z_t = \Phi_Q(\beta^s)d_t \quad \textbf{(5)}$$

From equation (4 & 5), the description of parameters are described in the below paragraph.

According to Mishra and Desai, and Shaukat et al. (Mishra & Desai, 2005; Shaukat et al., 2020), the general SARIMA model can be defined as:

$$\psi_p(\beta)\phi_p(\beta^s)\nabla^d\nabla_s^D z_t = \gamma_q(\beta)\Phi_Q(\beta^s)d_t \quad (6)$$

where p and q indicate parameters of the non-seasonal part, while P and Q indicate parameters of the seasonal part. Further, d is differencing parameter and associated with non-seasonal as well as D is associated with seasonal part. The notation s indicates the length of a season, z_t is current value and d_i stands for a set of uncorrelated random shocks. Moreover, the $\psi_p(\beta)$ and $\gamma_q(\beta)$ are non-seasonal AR and MA operators, whereas the $\phi_p(\beta^s)$ and $\Phi_Q(\beta^s)$ are seasonal operators respectively. Likewise, the notation ∇^d and ∇_s^D are non-seasonal and seasonal differencing operator. The construction of a stochastic model includes three steps such as identification, parameter estimation and diagnostic check.

The detail about model development is described in results section. The forecast package has been used on R version 3.6.1 for the time series modeling. We used (1,0,0) (2,1,1)12 model for SST forecasting.

3. Results

3.1. Statistical and climatology results

The minimum (Min), maximum (Max), mean, and standard deviation (SD) values of SST based on descriptive statistics were calculated for all 213 months images. We also practiced averages for descriptive statistics including minimum, maximum, MEAN, and STANDARD DEVIATION values of SST for each month (Table 1). Then, the "Mean SST" data sets for each month have been used for further analysis and also month/year wise SST monthly Mean graphical data in Figure 3 and time series in Figure S1 (S means Supplementary material). By using GIS, we summed all raster data sets month-wise that attests to the monthly spatial distribution of Sea surface temperature climatology from August 2002 – April 2020 (Figure 4).

Table S1 shows mean monthly values of SST in the study area. Table S2 highlights the warmer months during the study period from August 2002 to March 2022. May and September had the highest occurrences of warmer years, with four instances each, indicating these months typically experience elevated temperatures. June also showed notable warmth with three occurrences, while January, October, and November had fewer instances, suggesting they are generally cooler. The data reflects variability in warmth across different months, which could Table S2 identifies the hotter months with maximum temperatures nearing 40°C and provides details on their frequency and average temperatures. April and May emerge as the hottest months, each occurring 18 times and consistently showing mean temperatures above 29°C from 2003 to 2021. June also recorded high temperatures in four years (2003, 2010, 2019, and 2020). October had nine instances of extreme heat, while March, September, and November had fewer occurrences. Overall, the data indicates that 22.45% of the months analyzed experienced

Table 1. Descriptive statistics (Averages Monthly Indices) retrieved from the MODIS SST monthly images 2002 to 2020

Months	Min	Max	Mean	SD
January	0.122222	39.51028	27.18046	1.961827778
February	3.266667	39.66472	27.34973	2.1387
March	7.807778	39.67361	28.35566	2.075183333
April	6.545	39.75861	29.56817	1.660683333
May	4.877353	39.84147	29.69501	1.136258824
June	7.102059	39.86765	28.69206	1.501535294
July	10.38412	39.79706	27.71114	2.009970588
August	12.79528	39.80778	27.75962	2.114461111
September	11.1775	39.87778	28.28003	1.744538889
October	7.945278	39.74444	28.99306	1.076572222
November	3.864444	39.65778	28.78402	1.025894444
December	1.460556	39.45583	27.89507	1.573544444
Grand Total	6.445688	39.72142	28.35533	1.668264188

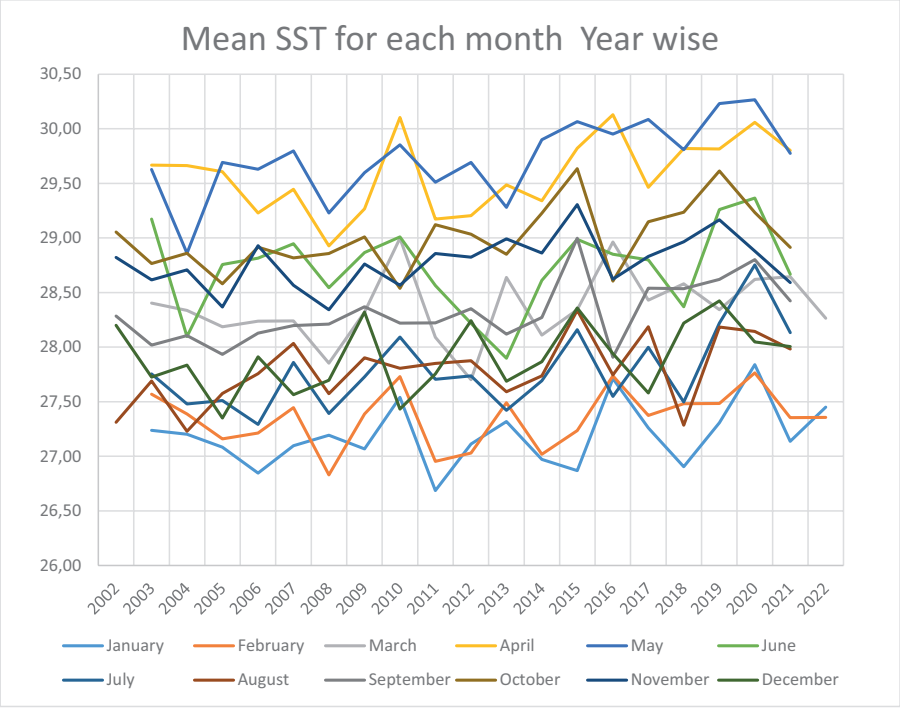

Figure 3. Monthly Mean Temperature °C Aug 2002 to March 2022

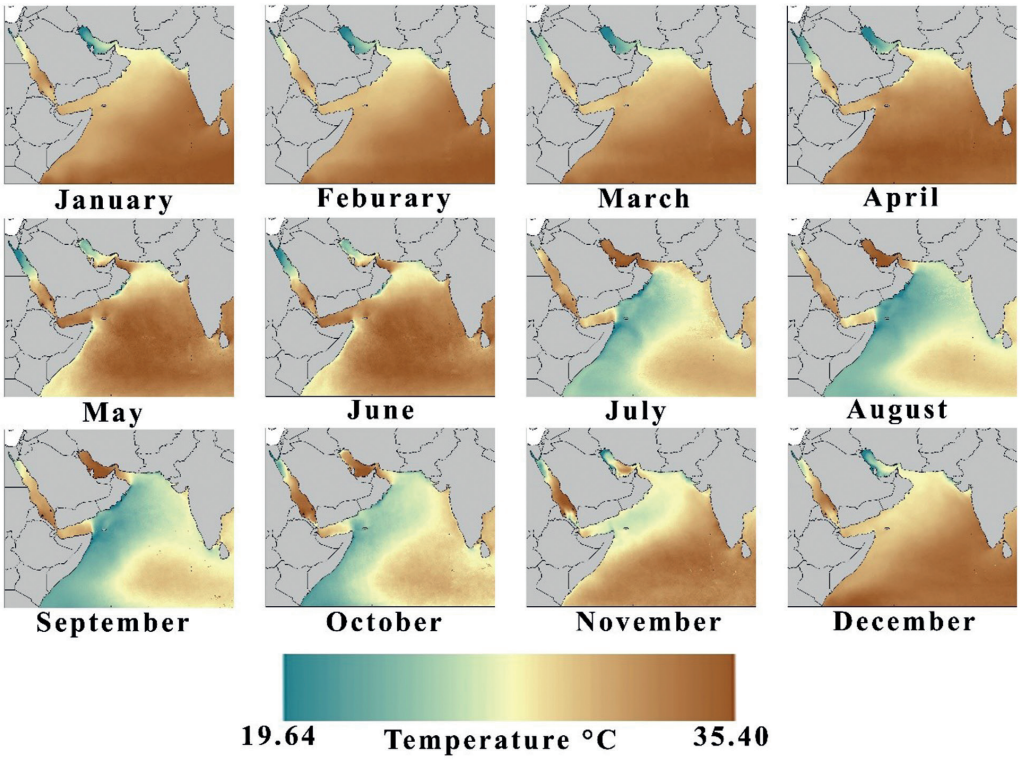

Figure 4. Inter-annual spatial distribution of sea surface temperature climatology during August 2002 – April 2020

warmer temperatures above 29°C, reflecting a significant trend towards increasing heat during this period.

Table S3 identifies the hotter months with maximum temperatures nearing 40°C and provides details on their frequency and average temperatures. April and May emerge as the hottest months, each occurring 18 times and consistently showing mean temperatures above 29°C from 2003 to 2021. June also recorded high temperatures in four years (2003, 2010, 2019, and 2020). October had nine instances of extreme heat, while March, September, and November had fewer occurrences. Overall, the data indicates that 22.45% of the months analyzed experienced warmer temperatures above 29°C, reflecting a significant trend towards increasing heat during this period.

3.2. Seasonal and Inter-Annual Results

Figure S2 displays inter-annual mean temperatures in a box plot format, highlighting evident seasonal variations with bimodal peaks. The monthly variation is characterized by a first peak in April-May and a second, slightly lower peak in October-November. Figure S3 illustrates yearly variations, showing minimum, maximum, mean, and standard deviation of SST from 2002 to 2022. Figure 5 shows the seasonal averages of spatially-averaged mean SST in the study area for four distinct periods: (a) December to February, (b) March to May, (c) June to August, and (d) September to November, covering the years 2002 to 2020. Figure 6 provides the annual average SST for each year during the study period, while Figure 7 displays the composite average SST over nearly 20 years, from August 2002 to April 2020.

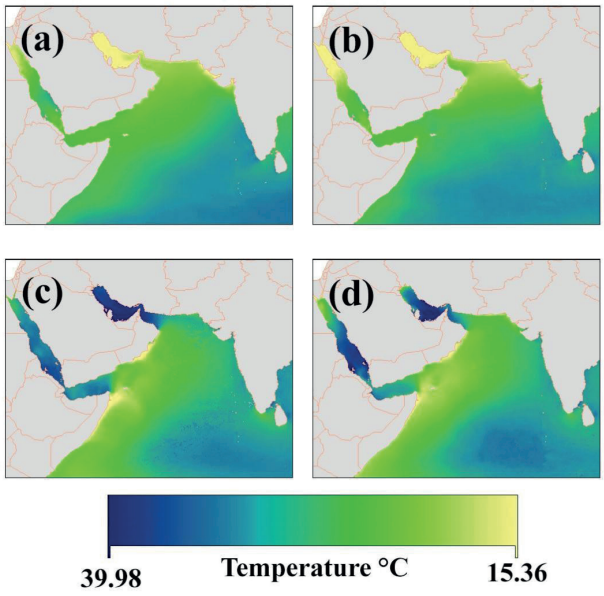

Figure 5. The inter-annual variation of spatially averaged Mean SST ((a) Dec to Feb (b)March to May (c) June to August (d) September to November from 2002 to 2020)

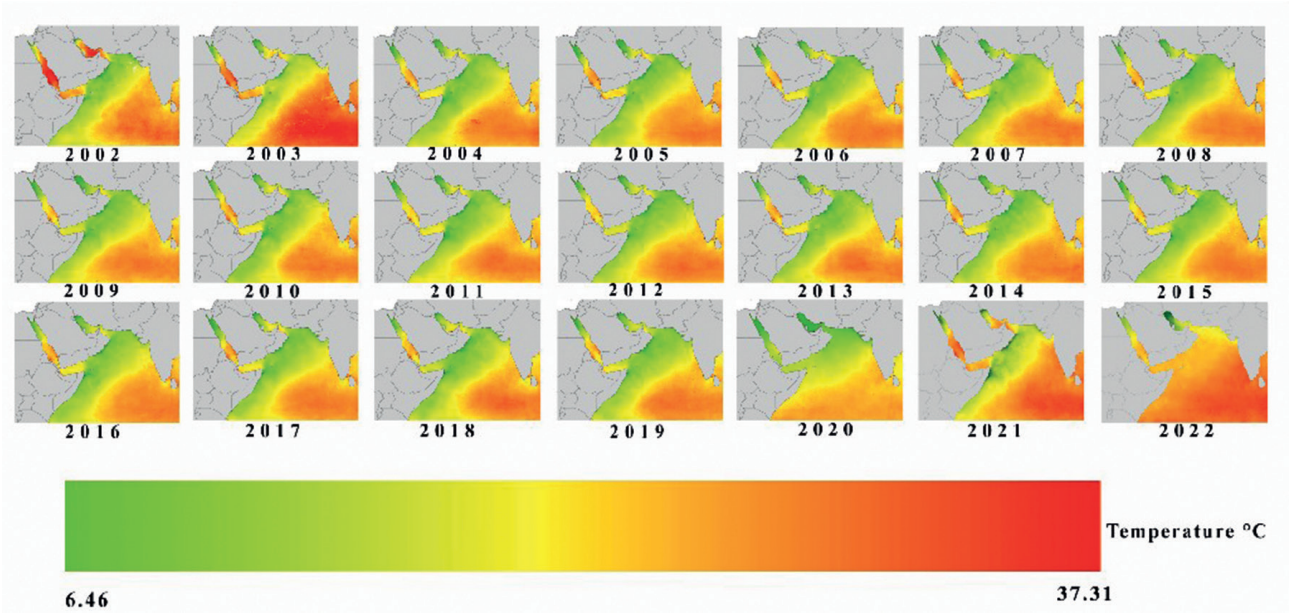

Figure 6. Year-wise annual averaged of SST during August 2002–April 2020

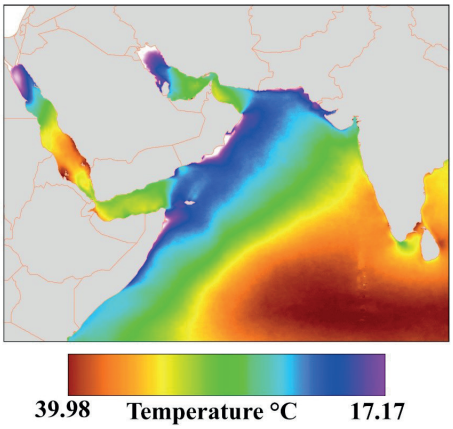

Figure 7. Spatial distribution of almost 20 years composite averaged SST during August 2002–April 2020

3.3. SST Anomaly and SST Normalized Anomaly

Figure 8 displays the SST anomaly during the study period. Overall, anomaly and recent trends show positive and increasing values. As we know that positive and rising SST anomaly indicates that the noted temperature is edging up and warmer than the earlier SST data. Figure 9 exhibits a standardized anomaly and mean temperature from 2002 to 2022. A standardized anomaly is thought more reliable for variation or anomaly studies. This also on rising trends implies a slight remodeling in SST means or climate change. Figures S4, S5 and S6 display Monthly Comparison of SST Anomaly and SST Normalized Anomaly from January to April, May to August, and September to December, respectively.

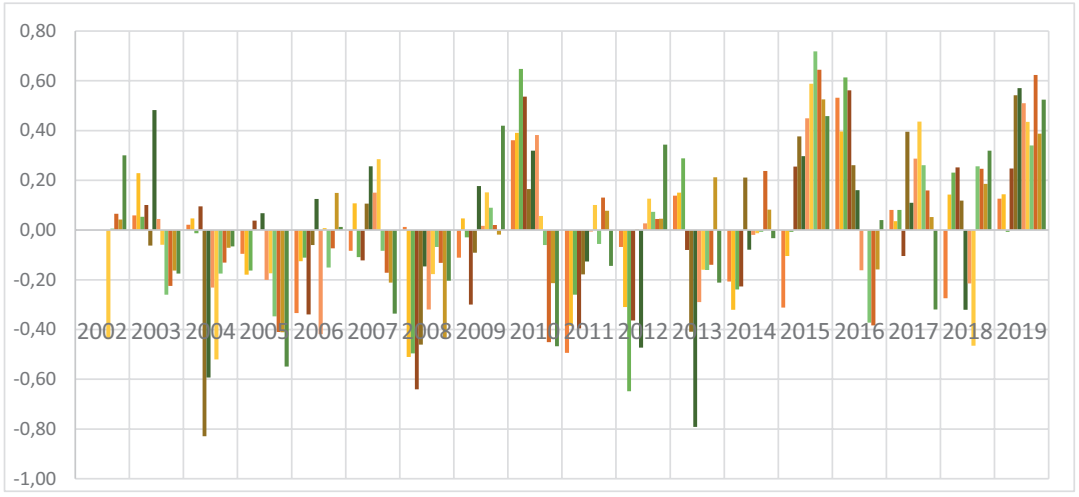

Figure 8. SST Anomaly during 2002 to 2020

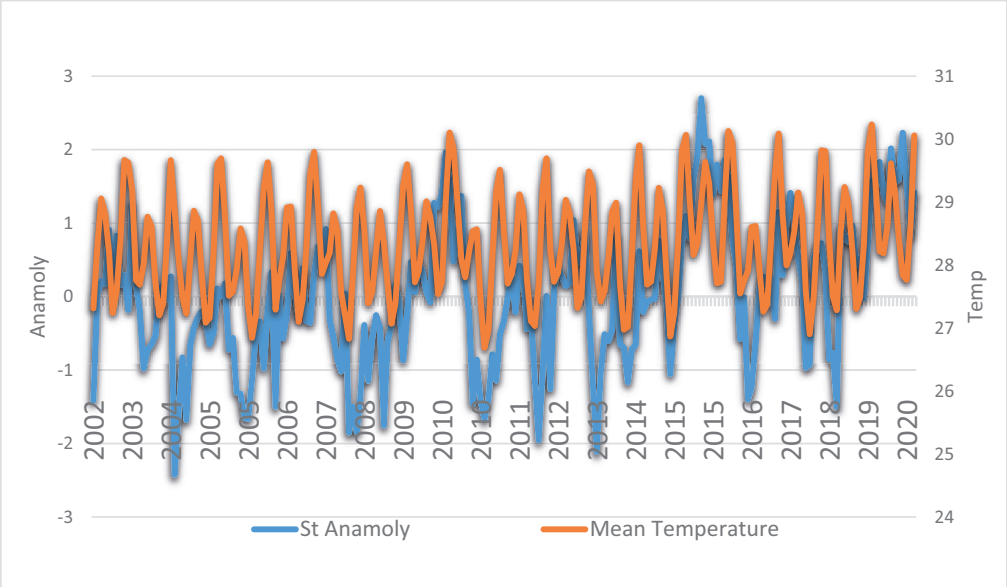

Figure 9. Standardize anomaly and mean temperature during 2002 to 2020

3.4. Coefficient of Variation of Annual and Seasonal SST

The coefficient of variation (CV) illustrates the magnitude of both monthly and inter-annual variability in Tables 2 and 3. The CV values for the month-wise and year-wise SST in the North Indian Ocean indicate significant variation among the mean SSTs of the study area. Notably, the most considerable variation in annual SST occurred in June, with a CV of 1.30%, followed by December (CV of 1.18%) and April (CV of 1.17%) as shown in Table 2.

In intra-annual or yearly variability the year 2020 exhibited the highest mean SST variability, with a CV of 3.72%. This was followed by 2015 (CV of 3.43%) and 2018 (CV of 3.39%), as detailed in Table 3. Overall, these variation metrics underscore the fluctuations in SST and may signify broader trends related to climate change.

Table 2. Month Wise coefficient of variation (CV)

Months	Mean Temp	Standard Deviation	(CV)
January	27.18	0.3	1.09
February	27.35	0.28	1.01
March	28.36	0.33	1.17
April	29.57	0.35	1.17
May	29.7	0.34	1.15
June	28.69	0.38	1.31
July	27.71	0.28	1.01
August	27.76	0.31	1.11
September	28.28	0.27	0.94
October	28.99	0.31	1.07
November	28.78	0.25	0.87
December	27.9	0.33	1.18

Table 3. Month Wise coefficient of variation (CV)

Year	Mean Temp	Standard Deviation	(CV)
2002	28.33	0.68	2.38
2003	28.35	0.82	2.9
2004	28.15	0.77	2.74
2005	28.15	0.89	3.15
2006	28.24	0.87	3.1
2007	28.33	0.81	2.87
2008	28.05	0.75	2.68
2009	28.38	0.76	2.69
2010	28.49	0.87	3.05
2011	28.21	0.88	3.12
2012	28.25	0.82	2.91
2013	28.23	0.78	2.76
2014	28.3	0.92	3.24
2015	28.68	0.99	3.44
2016	28.48	0.88	3.08
2017	28.48	0.86	3.01
2018	28.39	0.96	3.4
2019	28.72	0.91	3.16
2020	28.5711	1.06488	3.727122

3.5. SARIMA Forecasting with R

The average temperature time series from August 2002 to April 2020 has been used for the forecasting until April 2023 (Figure S7). In this regard, the time series plot of temperature is made for visualizing the time series components that are depicted in Figure S6 with R coding.

In the identification stage, the normality assumption of the temperature series is verified by the Shapiro Wilk (SW) test. Then, the Anderson Darling (AD) test is applied to check the stationary assumption of the time series.

Initially, the parameters of stochastic model are estimated by visualization of Autocorrelation Function (ACF) and Partial Autocorrelation Function (PACF) plot as described by Mishra and Desai (Mishra & Desai, 2005). Numerous parameter combinations were used to check the appropriateness of stochastic models. Their appropriateness is confirmed by the lowest value of Mean Absolute Error (MAE), Root Mean Square Error (RMSE) and Mean Absolute percentage Error (MAPE). Among all of appropriate stochastic models, the selection criteria for the best model is based on the lowest value of Akaike Information Criterion (AIC). The parameters of best-fitted model are estimated by Maximum Likelihood Estimation (MLE). The description of model fitting is described in Table 4.

Table 4 summarizes the results of a Seasonal Autoregressive Integrated Moving Average (SARIMA) model applied to temperature data, specifically the model SARIMA (1,0,0)(2,1,1)12SARIMA(1,0,0)(2,1,1)_{12}SARIMA(1,0,0)(2,1,1)12. The model achieved an Akaike Information Criterion (AIC) of -3.39, indicating a good fit, with a Mean Absolute Error (MAE) of 0.168067, a Root Mean Squared Error (RMSE) of 0.219935, and a Mean Absolute Percentage Error (MAPE) of 0.592403. These metrics suggest that the model accurately predicts temperature values. The Ljung-Box test statistic of 20, with a P-value of 0.2122, indicates no significant autocorrelation in the residuals, suggesting that the model effectively captures the underlying patterns in the data. Table 5 presents the estimated parameters of the SARIMA model, highlighting their statistical significance. The first parameter estimate of **0.6930** is statistically significant (P-value = 0.00000), indicating a strong positive effect on temperature predictions. The second parameter (-0.1822) and the third parameter (-0.1561) are not statistically significant, with P-values of 0.120879 and 0.134266, respectively. Conversely, the fourth parameter (-0.6866) is also highly significant (P-value = 0.00000), indicating its strong influence on the model. Overall, these results suggest that while some parameters significantly affect temperature, others do not contribute meaningfully to the model's predictive power.

Standard errors that are related to parameters are usually small as compared to parameter values are the clue of an estimated parameter are statistically significant and these parameters should be in the model (Shaukat et al., 2020 ; Misra & Desai, 2005). After this, the next step is to examine the residuals of best-fitted model. The residuals of best-fitted model should be uncorrelated and normally distributed. Therefore, the Ljung-Box test is applied to verify the absence of autocorrelation in the residuals. From Table 4, the p-value (0.2122) of Ljung-Box test is greater than commonly used level of significance (0.05). It is obvious indication of absence of autocorrelation and independently distributed. Further, the reliability of best-fitted model is confirmed by the visualization of ACF, histogram and time series plot of residuals that can be seen in Figure 10.

Table 5. Summary of SARIMA parameters

Parameter	Estimate	Standard Error	t statistic	P-value
ψ_1	0.6930	0.0516	13.42918	0.00000
ϕ_1	-0.1822	0.1174	-1.5511	0.120879
ϕ_2	-0.1561	0.1042	-1.49749	0.134266
Φ_1	-0.6866	0.1124	-6.11065	0.00000

From Figure 10 the time plot of residuals shows that the mean around the zero and equal variance over time. It can be observed from ACF plot that all spikes are within the limit which is an indication of white noise residuals. Moreover, the histogram suggests that the residuals follow a normal distribution. All required conditions are verified by residuals of the best-fitted SARIMA model. Therefore, the forecast from the SARIMA model for 36 months (blue line) along with a 95% confidence level are shown in Figure 11.

Table 6 provides the temperature forecast generated by the SARIMA model for the period from May 2020 to April 2023, including the predicted values alongside the 95% Upper Confidence Level (UCL) and Lower Confidence Level (LCL). The forecast indicates monthly temperature values, demonstrating fluctuations throughout the years. For instance, the forecast for March 2021 is 28.51°C, with a confidence interval ranging from 27.89°C to 29.12°C, reflecting a relatively stable prediction. The highest forecasted temperature occurs in May 2022, with a predicted temperature of 30.01°C, and the UCL is 30.63°C, suggesting a peak in temperature during that month.

Table 4. Model Summary

Variable	Model	Parameter	AIC	MAE	RMSE	MAPE	Ljung-Box Test		
							Statistic	df	P-value
Temperature	SARIMA	(1,0,0) (2,1,1)12	- 3.39	0.168067	0.219935	0.592403	0.592403	20	0.2122

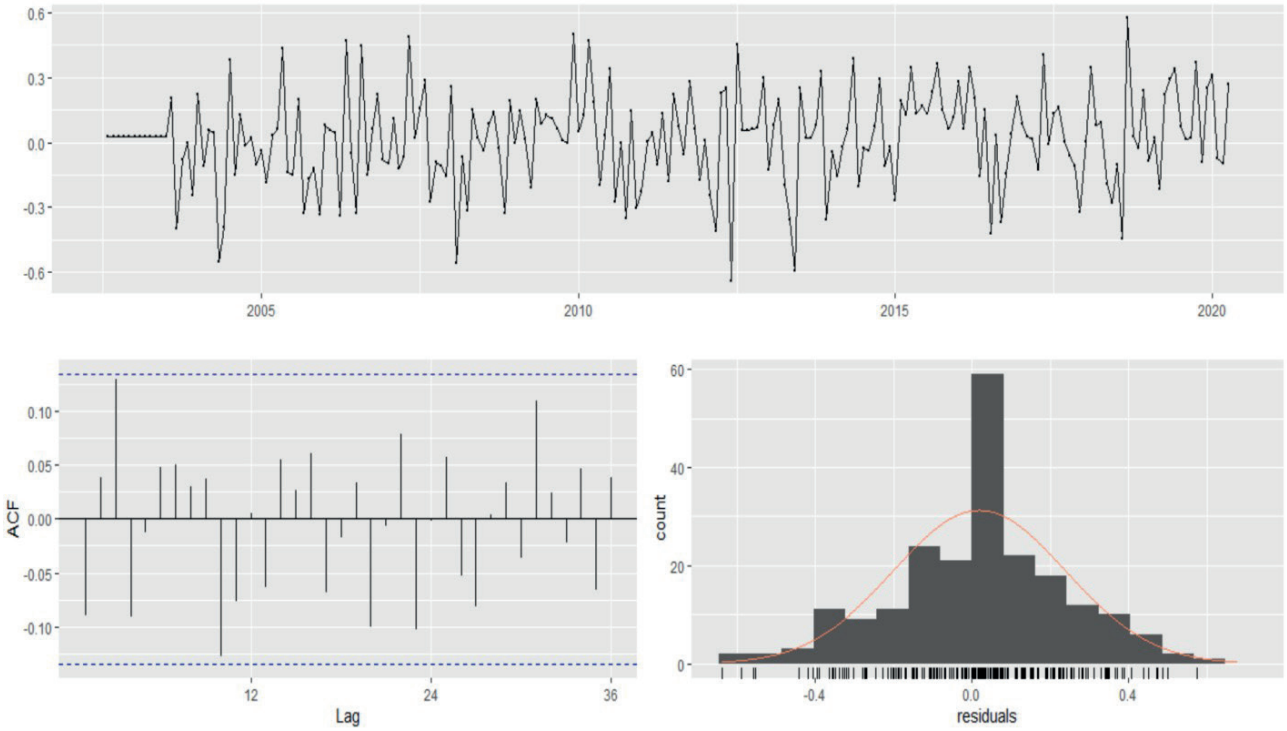

Figure 10. Diagnostic check of SARIMA model

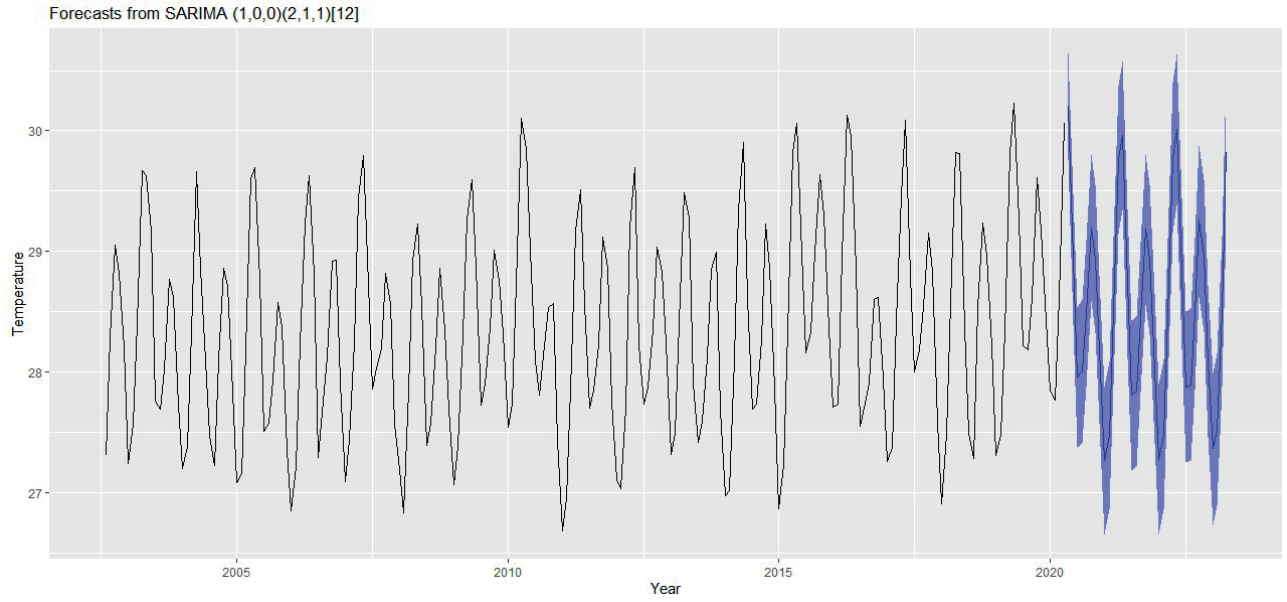

Figure 11. Temperature Forecast plot

The forecasted temperatures indicate a general trend of variability, with higher temperatures in late spring and early summer months, such as April and May, and cooler temperatures during winter months like January and February. For example, the forecast for April 2023 is 29.82°C, with a confidence interval between 29.19°C and 30.44°C, suggesting consistency in elevated temperatures as the season's transition. The inclusion of UCL and LCL provides a statistical confidence range, offering insights into the expected range of temperature values, which is crucial for understanding potential climate variability and its implications.

Table 6. Represents the temperature forecast from May 2020 to April 2023 with 95% Upper Confidence Level (UCL) and Lower Confidence Level (LCL)

Year	Month	Forecast	LCL	UCL
2021	Mar	28.50751	27.89235	29.12267
2021	Apr	29.75882	29.14361	30.37403
2021	May	29.96369	29.3452	30.58219
2021	Jun	28.73232	28.11225	29.35239
2021	Jul	27.80666	27.18584	28.42748
2021	Aug	27.83943	27.21825	28.46061
2021	Sep	28.45541	27.83405	29.07676
2021	Oct	29.18298	28.56154	29.80442
2021	Nov	28.92857	28.30709	29.55005
2021	Dec	28.02775	27.40626	28.64925
2022	Jan	27.27678	26.65527	27.89828
2022	Feb	27.47647	26.85496	28.09798
2022	Mar	28.48022	27.85871	29.10174
2022	Apr	29.77232	29.1508	30.39383
2022	May	30.00955	29.38515	30.63395
2022	Jun	28.81861	28.19283	29.44438
2022	Jul	27.8742	27.24776	28.50064
2022	Aug	27.89695	27.2702	28.52371
2022	Sep	28.48138	27.85447	29.10829
2022	Oct	29.25011	28.62313	29.8771
2022	Nov	28.96583	28.33881	29.59285
2022	Dec	28.08854	27.4615	28.71558
2023	Jan	27.36421	26.73716	27.99125
2023	Feb	27.52128	26.89423	28.14833
2023	Mar	28.50288	27.87583	29.12993
2023	Apr	29.81667	29.18962	30.44372

4. Discussion

Ocean variables play vital roles in global weather and climate systems. Sea surface temperature (SST) is especially significant for oceanic processes and marine life. Changes in SST patterns and seasonal variations affect the sustainability of marine ecosystems, including coral reefs, which are key indicators for assessing climate change impacts. SST has infinite significant applications: it superintends vitality trade between the world's environment and seas, controlling long haul atmosphere, typhoon track and power, and nearby climate. Sea surface temperature (SST) indicates the highest mixed layer of the sea, generally just barely a few several meters thick. Information on past SST fluctuation is meaningful as it lets us see how the sea acts amid environmental change; it allows us to approve mathematical climate models and evaluate the significance of current climate change (Belkin & O'Reilly, 2009). Temperature affects a range of thermodynamic, metabolic, and biological processes that leave their signature in the geological record (Zachos et al., 2003). Worldwide mean SST has ascended from decade-to-decade since the 1970s, with implications for worldwide climate examples and maritime biological systems (Meier et al., 2019). Most striking is the expanding recurrence of mass blanching occasions of coral reefs. Ongoing exploration introduces that sea heat has risen drastically over the previous decade, hinting the potential for warming water in the Indian Ocean to influence the Indian rainstorm, one of the most significant atmospheric designs on the planet. The global average SST rise of about 0.7°C over the same period. Most of this temperature rise is associated with anthropogenic emissions. SST is a central atmosphere variable for understanding the atmosphere framework and assessing the succeeding climatic change (Elepathage et al., 2020; Roxy et al., 2020).

There are many interpretations for SST variation, one of the prominent reasons is monsoon annual cycle within that the wind systems uniquely reverse its direction, also coastal and local breeze at a smaller scale. The Indian monsoon holds an annual cycle within which the winds completely reverse their direction, and thus, we may address the summer and winter monsoon (Graham & Barnett, 1987; Gnanaseelan et al., 2017). These monsoons are comparable to the coastal circulation or breeze but on a much larger scale. During summer, the Indian subcontinent warms up, makes incredible convection, and huge scope wind current inrushes to supplant the rising air masses. This is known as the Southwest Monsoon, characterized by winds rushing from the southwest, over the Arabian Sea. These breezes get enormous sums of dampness that is abandoned over the land as covering downpours. During winter, notwithstanding, the continent cools down faster than the Ocean, and thus the convection occurs over the warmer ocean. The replacement proceeds from the northeast and is known as the Northeast Monsoon (Zachos et al., 2003; Roxy et al, 2020). The circulation in the North Indian Ocean is peculiar in many ways, especially it improves with the season. Both, the southwest and the northeast, monsoons have a deep-felt effect on the ocean circulation, driving the extraordinary Somali Current (Hu & Fedorov, 2019). El Niño Southern Oscillation (ENSO) is a known linked for ocean-atmosphere model of intra-annual variability with a periodicity of about 4–7 years. El Niño is the positive phase of ENSO, characterized by irregular surface warming of eastern and central equatorial Pacific, lasting for several months. The negative phase with cooler (than normal) SST in the eastern equatorial Pacific is called La Niña. There are numerous indices to quantify the strength, nature, and duration of El Niño based on the anomalous SST over different regions

of eastern and central equatorial Pacific.Indian Ocean SSTs have a role in developing the surface air temperatures over the Indian subcontinent that may vary (Kug & Kang, 2006).

Rising ocean temperatures have also occurred in situations of marine heatwaves in the Indian Ocean. Oceangoing heatwaves are similar to heat waves over the land, with periods of remarkably high ocean temperatures that endure for days to months. Beyond the regional climate, Indian Ocean warming has global and remote consequences. The Indian Ocean has contributed to more than 21% of the global oceanic heat uptake over the last two decades and presented securely to the temporary slowdown in global warming from 1998–2013. Warming in the Indian Ocean and associated deep convection is observed to trigger droughts in South America and marine heatwaves in the adjacent South Atlantic (Cheng et al., 2016; Cheng et al., 2017; Pandey et al., 2024; Wang et al., 2024a; Wang et al., 2024b).

This study advances the understanding of sea surface temperature (SST) variability by connecting observed changes in the Indian Ocean to major global climate drivers, including climate change, El Niño/La Niña events, and the Indian monsoon, supported by relevant data and prior research. These links provide critical context and highlight the study's global relevance. The findings also point to significant ecological implications, particularly for coral reef health and ocean circulation, emphasizing the wider environmental impact of SST trends. The understandings expanded by this study can inform regional climate adaptation strategies, support sustainable marine resource management, and improve short-term forecasting to mitigate risks to coastal ecosystems and fisheries.

5. Conclusions

Remote sensing originated MODIS SST products have been successively adopted for assessment of SST dynamics and short term forecasting. Tis study explains the spatial patterns, trends, and temporal changes in sea surface temperature for approximately two decades. The annual SST trend is slightly on the rise. Inter-annually, May is the hottest month. Bimodal variation has been seen first in April, May months, and then in Sep-Oct. The marine climate and its influence on the ecosystem are an important matter for both environmental managers and members of the fishing industry, as well as for the society in general. The results achieved in this study strengthen the value of satellite data as a tool to study the spatial and temporal variability of SST in the Indian Ocean. SST patterns over 20 years highlight the significance of regional assessments for determining the rate and timing of warming at local and regional scales and the necessity for attention in extrapolating regional implications from global patterns. Moreover, the observed rising trend and forecasts can support decision-making aimed at reducing risks to marine and ecological systems.

Author Contributions

Conceptualization, I.A.K.; Data curation, I.A.K.; Writing, I.A.K., A. H .L, M.H.A., H.V, I.Z.; Review & editing, I.A.K, A. H .L, M.H.A, H.V.S.I and I Z.

Funding: This research received no external funding.

Conflicts of Interest: The authors declare no conflict of interest.

Acknowledgment

"The data used in this were acquired as part of the activities of NASA's Science Mission Directorate, and are archived and distributed by the Goddard Earth Sciences (GES) Data and Information Services Center (DISC)". "Analyses and visualizations used in this paper were produced with the Giovanni online data system, developed and maintained by the NASA GES DISC." We also acknowledge the MODIS mission scientists and associated NASA personnel for the production of the data used in this research effort.

References

Alonso del Rosario J.J., Vidal Pérez J.M. & Blázquez Gómez E., 2019, On the prediction of upwelling events at the Colombian Caribbean coasts from MODIS-SST imagery. Sensors, 19(13), 2861.

Beaugrand G., 2004, The North Sea regime shift: evidence, causes, mechanisms and consequences. Progress in Oceanography, 60(2-4): 245-262.

Belkin I.M. & O'Reilly J.E., 2009, An algorithm for oceanic front detection in chlorophyll and SST satellite imagery. Journal of Marine Systems, 78(3): 319-326.

Box G.E.P., Jenkins G.M. & Reinsel G.C., 1994, Time series analysis, forecasting and control. Englewood Cliffs.

Box G.E.P. & Jenkins G.M., 1970, Timeseries analysis, forecasting and control. Holden-Day, San Francisco, CA.

Chen P., Niu A., Liu D., Jiang W. & Ma B., 2018, Timeseries forecasting of temperatures using SARIMA: An example from Nanjing. In: IOP Conference Series: Materials Science and Engineering, 394(5), pp. 1-7.

Chen C.F., Chang Y.H. & Chang Y.W., 2009, Seasonal ARIMA forecasting of inbound air travel arrivals to Taiwan. Transportmetrica, 5(2): 125-140.

Cheng L., Trenberth K.E., Fasullo J., Boyer T., Abraham J. & Zhu J., 2017, Improved estimates of ocean heat content from 1960 to 2015. Science Advances, 3(3), e1601545.

Cheng L., Trenberth K.E., Palmer M.D., Zhu J. & Abraham J.P., 2016, Observed and simulated full-depth ocean heat-content changes for 1970–2005. Ocean Science, 12(4): 925-935.

Choi Y., Kim D., Cho S. & Kim T.W., 2019, Southeastern Yellow Sea as a sink for atmospheric carbon dioxide. Marine Pollution Bulletin, 149, 110550.

Elepathage T.S. & Tang D., 2020, Relationships among SST variability, physical, and biological parameters in the northeastern Indian Ocean. Atmosphere-Ocean, 1-4.

Embury O., Merchant C.J., Good S.A., Rayner N.A., Høyer J.L., Atkinson C., et al., 2024, Satellite-based time-series of sea-surface temperature since 1980 for climate applications. Scientific Data, 11(1), 326.

Gladkova I., Ignatov A., Shahriar F., Kihai Y., Hillger D. & Petrenko B., 2016, Improved VIIRS and MODIS SST imagery. Remote Sensing, 8(1): 79.

Gnanaseelan C., Roxy M.K. & Deshpande A., 2017, Variability and trends of sea surface temperature and circulation in the Indian Ocean. In: Observed Climate Variability and Change over the Indian Region, pp. 165-179, Springer, Singapore.

Goswami K., Hazarika J. & Patowary A.N., 2017, Monthly temperature prediction based on ARIMA model: A case study in Dibrugarh Station of Assam, India. International Journal of Advanced Research in Computer Science, 8(8).

Graham N.E. & Barnett T.P., 1987, Sea surface temperature, surface wind divergence, and convection over tropical oceans. Science, 238(4827): 657-659.

Harrison P.J., Piontkovski S. & Al-Hashmi K., 2017, Understanding how physical-biological coupling influences harmful algal blooms, low oxygen and fish kills in the Sea of Oman and the Western Arabian Sea. Marine Pollution Bulletin, 114(1): 25-34.

Hu S., Fedorov A.V., 2019, Indian Ocean warming can strengthen the Atlantic meridional overturning circulation, Nature Climate Change, 9(10): 747-751.

Ji C., Zhang Y., Cheng Q., Tsou J., Jiang T. & San Liang X., 2018, Evaluating the impact of sea surface temperature (SST) on spatial distribution of chlorophyll-a concentration in the East China Sea. International Journal of Applied Earth Observation and Geoinformation, 68: 252-261.

Karagali I., Høyer J. & Hasager C., 2012, SST diurnal variability in the North Sea and the Baltic Sea. Remote Sensing of Environment, 121: 159-170.

Khan I.A., Ghazal L., Arsalan M.H., Siddiqui M.F. & Kazmi J.H., 2015, Assessing spatial and temporal variability in phytoplankton concentration through chlorophyll-a satellite data: A case study of northern Arabian Sea. Pak. J. Bot., 47(2): 797-805.

Kilpatrick K.A., Podestá G., Walsh S., Williams E., Halliwell V., Szczodrak M., et al., 2015, A decade of sea surface temperature from MODIS. Remote Sensing of Environment, 165: 27-41.

Kug J.S. & Kang I.S., 2006, Interactive feedback between ENSO and the Indian Ocean. Journal of Climate, 19(9): 1784-1801.

Malik H.Y., 2012, Strategic importance of Gwadar Port. Journal of Political Studies, 19(2).

McWilliams J.P., Côté I.M., Gill J.A., Sutherland W.J. & Watkinson A.R., 2005, Accelerating impacts of temperature-induced coral bleaching in the Caribbean, Ecology, 86(8): 2055-2060.

Meier H.E., Eilola K., Almroth-Rosell E., Schimanke S., Kniebusch M., Höglund A., et al., 2019, Disentangling the impact of nutrient load and climate changes on Baltic Sea hypoxia and eutrophication since 1850. Climate Dynamics, 53(1-2): 1145-1166.

Minnett P.J., Alvera-Azcárate A., Chin T.M., Corlett G.K., Gentemann C.L., Karagali I., et al., 2019, Half a century of satellite remote sensing of sea-surface temperature. Remote Sensing of Environment, 233, 111366.

Minnett P.J., Brown O.B., Evans R.H., Key E.L., Kearns E.J., Kilpatrick K., et al., 2004, Sea-surface temperature measurements from the Moderate-Resolution Imaging Spectroradiometer (MODIS) on Aqua and Terra. In: IGARSS 2004 IEEE International Geoscience and Remote Sensing Symposium, Vol. 7, pp. 4576-4579, IEEE.

Mishra A.K. & Desai V.R., 2005, Drought forecasting using stochastic models, Stochastic Environmental Research and Risk Assessment, 19(5): 326-339.

Nandkeolyar N., Raman M. & Kiran G.S., 2013, Comparative analysis of sea surface temperature pattern in the eastern and western gulfs of Arabian Sea and the Red Sea in recent past using satellite data. International Journal of Oceanography, 2013.

Osborne E.B., Thunell R.C., Gruber N., Feely R.A. & Benitez-Nelson C.R., 2020, Decadal variability in twentieth-century ocean acidification in the California Current Ecosystem. Nature Geoscience, 13(1): 43-49.

Pandey V.K., Das B.K., Singh Y. & Srivastav S., 2024, Exploring temporal and spatial SST patterns and their impact in the Arabian Sea: Insights from the regional ocean modeling system. Continental Shelf Research, 275, 105224.

Pastor F., Valiente J.A. & Palau J.L., 2019, Sea surface temperature in the Mediterranean: Trends and spatial patterns (1982–2016). In: Meteorology and climatology of the Mediterranean and Black Seas, Birkhäuser, Cham, pp. 297-309.

Putra R.D., Suhana M.P., Kurniawan D., Abrar M., Siringoringo R.M., Sari N.W., et al., 2019, Detection of reef scale thermal stress with Aqua and Terra MODIS satellite for coral bleaching phenomena. In: AIP Conference Proceedings, 2094(1), 020024.

Quan-jun H., 2009, Realization of SST retrieval from Modis1B data using IDL. Journal of Tropical Meteorology, 25(2).

Raitsos DE, Pradhan Y, Brewin RJ, Stenchikov G & Hoteit I., 2013, Remote sensing the phytoplankton seasonal succession of the Red Sea. PloS One, 8(6), e64909.

Rayner N.A., Parker D.E., Horton E.B., Folland C.K., Alexander L.V., Rowell D.P., et al., 2003, Global analyses of sea surface temperature, sea ice, and night marine air temperature since the late nineteenth century. Journal of Geophysical Research: Atmospheres, 108(D14).

Roxy M.K., Gnanaseelan C., Parekh A., Chowdary J.S., Singh S., Modi A., et al., 2020, Indian Ocean warming. In: Assessment of Climate Change over the Indian Region, Springer, Singapore, pp. 191-206.

Saeedi H., Reimer J.D., Brandt M.I., Dumais P.O., Jażdżewska A.M., Jeffery N.W., et al., 2019, Global marine biodiversity in the context of achieving the Aichi Targets: ways forward and addressing data gaps. PeerJ, 7, e7905.

Saleem N., Khan I.A. & Lasi A., 2023, Monitoring the spatiotemporal variations in sea surface temperature along the coastal waters of Pakistan. Environmental Monitoring and Assessment, 195, 342.

Sasaki H., Ishizaka J. & Fujiki T., 2017, Spatiotemporal characteristics of the upwelling off the southern coast of Java. Geophysical Research Letters, 44(3): 1359-1367.

Schneider A., Hook S.J., Jiang L. & Liu X., 2022, Inter-comparison of satellite-based sea surface temperature products for monitoring coral reef thermal stress. Remote Sensing, 14(18), 4501.

Sellers P, Hall F, Tucker C, Justice C, Dazlich D, Gilman J, et al., 1996, Global terrestrial biophysical data set. NASA Technical Memorandum.

Smith T.M. & Reynolds R.W., 2003, Extended reconstruction of global sea surface temperature based on COADS data (1854–1997). Journal of Climate, 16(10): 1495-1510.

Song Y., Zhao X., Wang H., Cao S., Zhang Y., Zhang H., et al., 2022, Evaluation of SST products and its application in coastal waters monitoring. Remote Sensing, 14(6), 1290.

Sun X., Guan X., Liu J., 2016, Analysis of spatial and temporal variation of sea surface temperature in the South China Sea, Remote Sensing, 8(2): 133.

Thiault L., Le Borgne R., Andréfouët S. & Claudet J., 2019, Marine heatwaves threaten global biodiversity hotspots. Global Change Biology, 25(3): 891-902.

Thompson W.R., Pollard D., Gordon A., Wilson S., Pease C. & Royer D.L., 2020, Reconstructing sea surface temperature changes since the last glacial maximum. Geophysical Research Letters, 47(3), e2019GL085286.

Tomczak M., 1999, Sea surface temperature trends in the Tasman Sea and adjacent South Pacific Ocean. Marine and Freshwater Research, 50(5): 723-733.

Wang C., & Enfield D.B., 2001, The tropical Western Hemisphere warm pool. Geophysical Research Letters, 28(8): 1635-1638.

Wang Y., Wang D. & Wang M., 2023, The spatiotemporal pattern and variation of sea surface temperature in the East China Sea. Remote Sensing, 15(4), 1026.

Wang Z., Wu D., Chen Y. & Xie Y., 2021, Analysis of oceanographic parameters with MODIS data: a case study in the South China Sea. Remote Sensing, 13(18), 3705.

Wei J., Li Z., Yuan J., Du Y. & Chen D., 2019, Estimating coastal sea surface temperature using a combination of satellite data and machine learning methods. Remote Sensing, 11(11), 1323.

Wilson C., Johnson G.A. & Tivey M.K., 2019, Oceanographic impacts of submarine volcanism on hydrothermal vent ecosystems. Geology, 47(6): 525-528.

Wu Z., Liu Y., Du H., Fang Z. & Qin B., 2018, Impact of sea surface temperature on chlorophyll-a concentration in Lake Taihu. Science of the Total Environment, 636: 1489-1498.

Yang S., Wang Y. & Huang S., 2017, Forecasting monthly sea surface temperature anomalies using a hybrid SARIMA and neural network model. Ocean Engineering, 142: 1-8.

Zhou X., Shi P., Song X. & Li X., 2020, Sea surface temperature prediction using SARIMA model: a case study in the Bohai Sea. Journal of Ocean University of China, 19(1): 77-86.